UNIVERSITY OF LEEDS

This is a repository copy of *Intracoronal stress transfer through enamel following RBC photopolymerisation: A synchrotron X-ray study*.

White Rose Research Online URL for this paper:
http://eprints.whiterose.ac.uk/134538/

Version: Accepted Version

Article:
Al-Jawad, M, Addison, O, Sirovica, S et al. (4 more authors) (2018) Intracoronal stress transfer through enamel following RBC photopolymerisation: A synchrotron X-ray study. Dental Materials, 34 (10). pp. 1426-1439. ISSN 0109-5641

https://doi.org/10.1016/j.dental.2018.07.005

Reuse
Items deposited in White Rose Research Online are protected by copyright, with all rights reserved unless indicated otherwise. They may be downloaded and/or printed for private study, or other acts as permitted by national copyright laws. The publisher or other rights holders may allow further reproduction and re-use of the full text version. This is indicated by the licence information on the White Rose Research Online record for the item.

Takedown
If you consider content in White Rose Research Online to be in breach of UK law, please notify us by emailing eprints@whiterose.ac.uk including the URL of the record and the reason for the withdrawal request.

White Rose university consortium
Universities of Leeds, Sheffield & York

eprints@whiterose.ac.uk
https://eprints.whiterose.ac.uk/

Figure 1

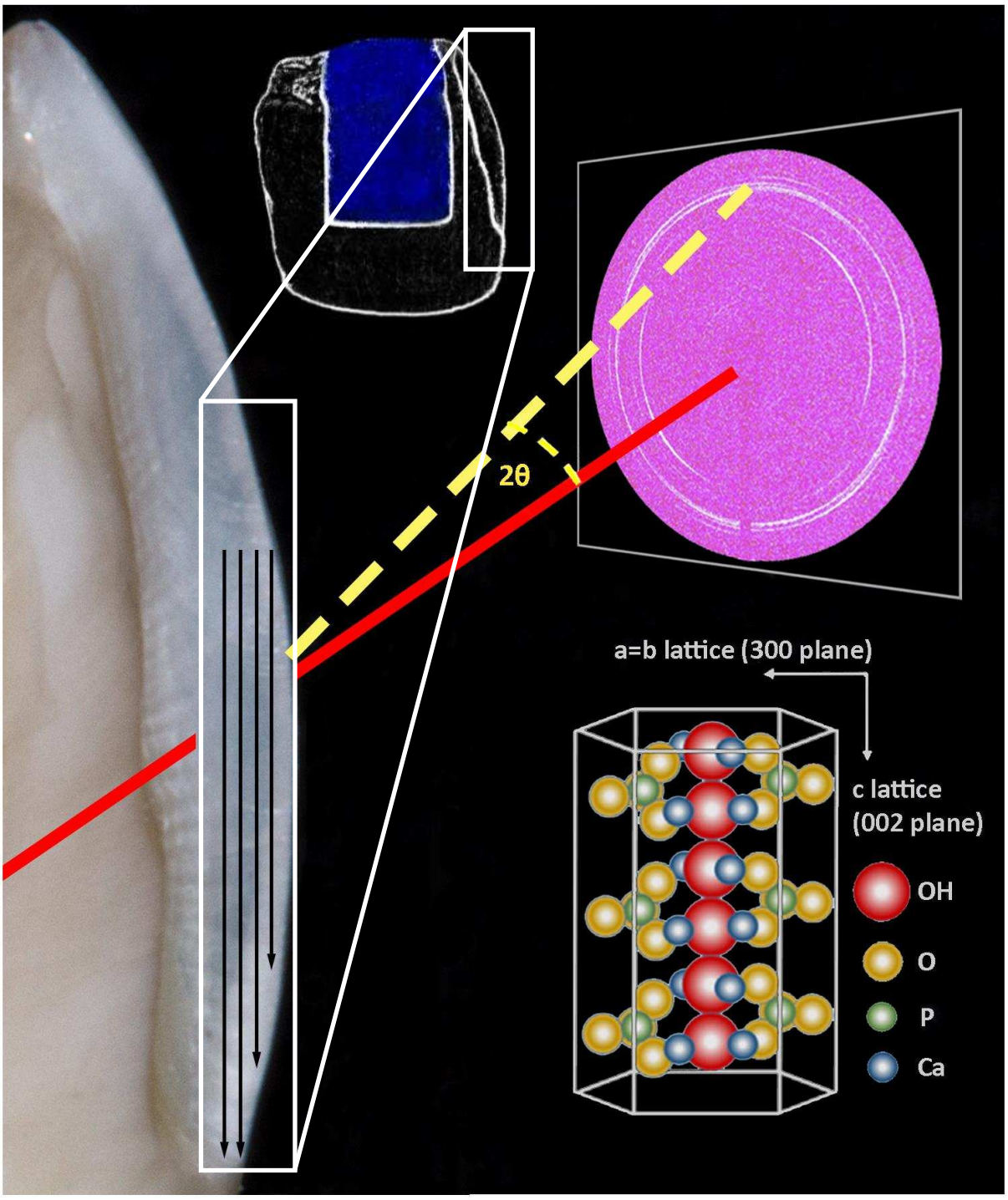

Figure 1. Experimental setup at the B16 beamline (Diamond Light Source) with an example 2D diffraction image. A vertical fin in the outer enamel of a pre-molar tooth is mapped by successive XRD line scan measurements (tracks 1-4, left to right, separated by 0.1mm). Additional single line scan measurements, taken approximately between tracks 2 and 3, were used to acquire sufficient statistics for each irradiance regime on other tooth specimens. Diffraction images are collected at each point by a detector behind and in the path of the tooth specimen in transmission geometry, and used to calculate crystallographic lattice parameters, preferred orientation and texture for hydroxyapatite (lower inset) within the tooth enamel. To the left of the vertical fin is the cavity wall to which the composite (shown in blue) was bonded (upper inset).

Figure 2

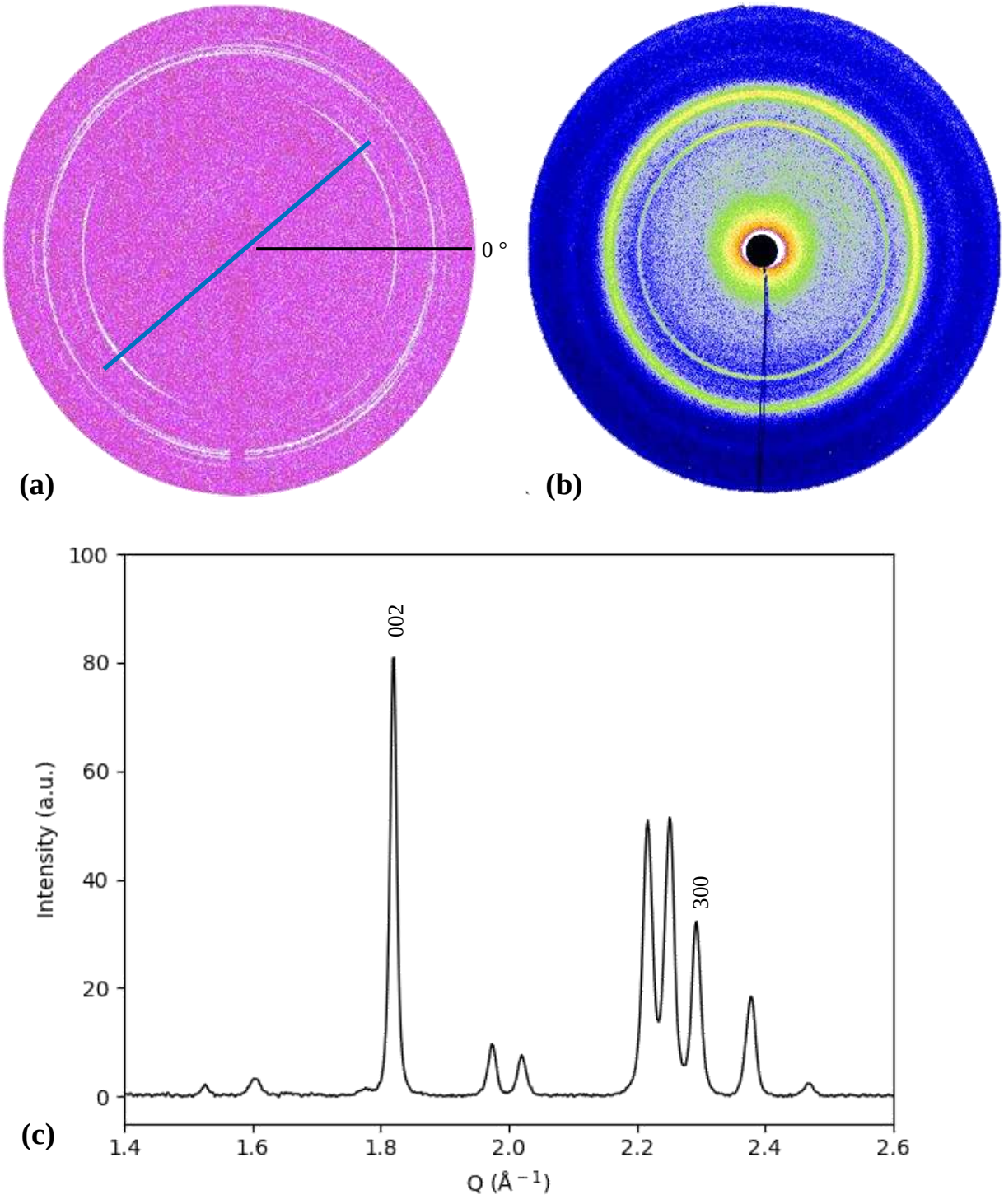

Figure 2. (a) The intensity of the (002) Debye diffraction ring varies as a function of azimuthal angle. This is indicative of texture (preferred orientation) within the hydroxyapatite phase of enamel. Preferred orientation is defined from 0° which points east on the detector face, increasing azimuthally in the anti-clockwise direction The most pronounced direction of crystallite alignment is marked by the blue line. In **(b)** for illustrative purposes only, a diffraction pattern with uniform intensity around the (002) ring is shown demonstrating little or no texture (hydroxyapatite 2DXRD pattern of cortical bone). **(c)** A 1-D diffraction pattern with the (002) and (300) reflections located at 2θ=10.29° and 13.15° respectively.

Figure 3

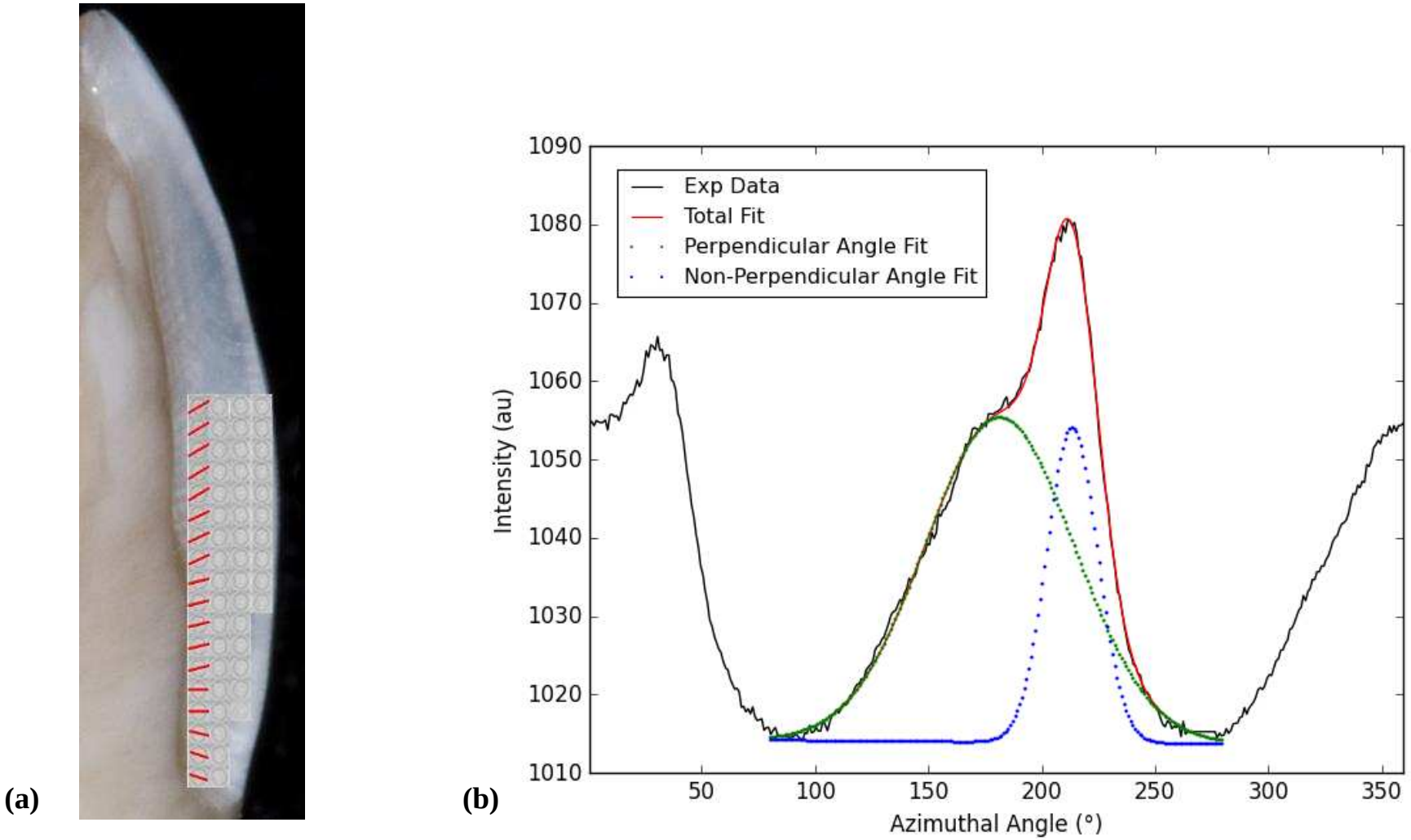

Figure 3. (a) A composite image showing individual 2-D diffraction patterns, for each measurement along a track (tracks 1-4, left to right), superimposed on to a schematic of a tooth enamel fin. Bisection of the (002) diffraction rings through points of greatest intensity yields the approximate direction of preferred orientation, which are shown as red lines. **(b)** Azimuthal integration of the (002) diffraction ring, followed by deconvolution, shows a bimodal distribution, indicating that two directions of crystallite/prismatic orientation exist within the tooth enamel.

Figure 4

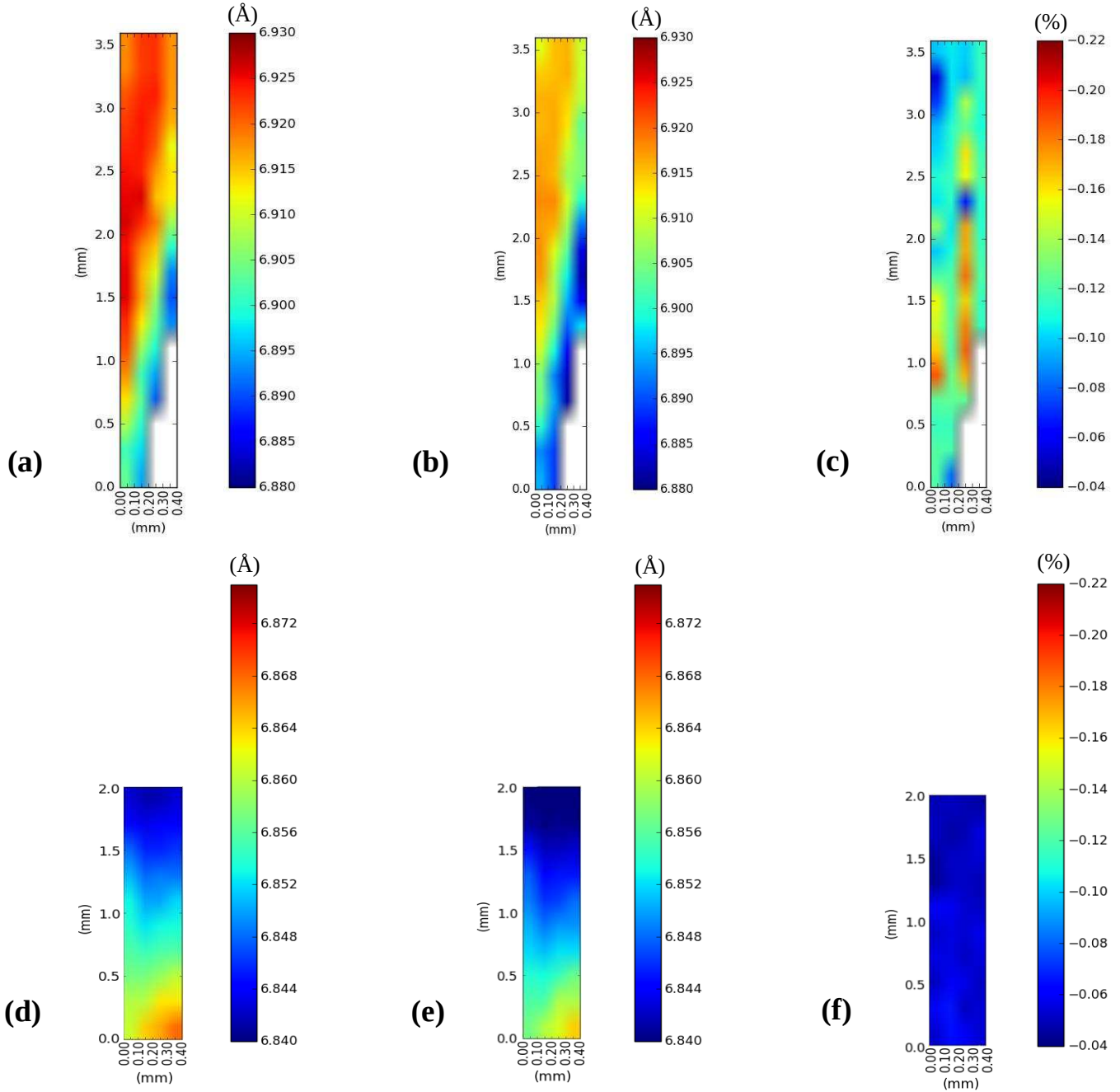

Figure 4. Contour maps for the c-lattice parameter over the scanned region of a given enamel 'fin' before and after LED and QTH curing. A colour scale-bar is shown to the right of each contour map. The cavity wall is located to the left of each contour map. **(a)** LED before. **(b)** LED after. **(c)** LED % lattice strain; **(d)** QTH before. **(e)** QTH after .**(f)** QTH % lattice strain.

Figure 5

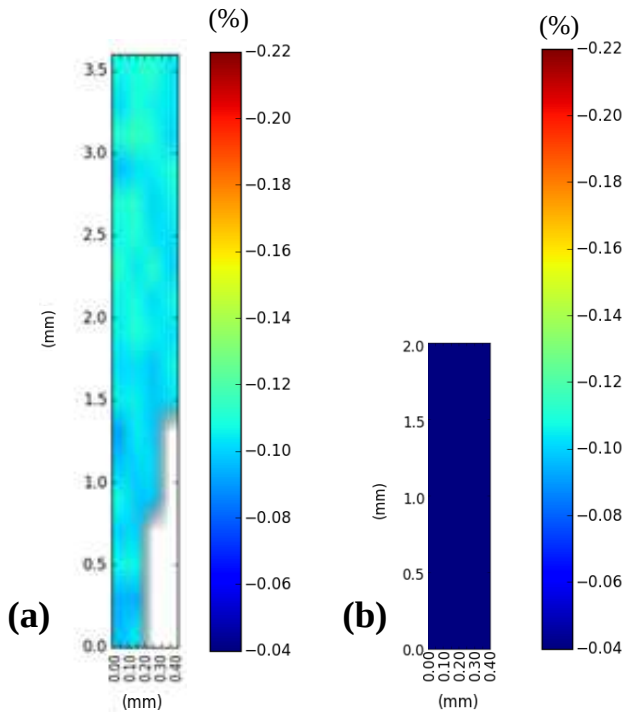

Figure 5. Crystallographic strain along the a axis for **(a)** high and **(b)** low irradiance photo-polymerization protocols.

Figure 6

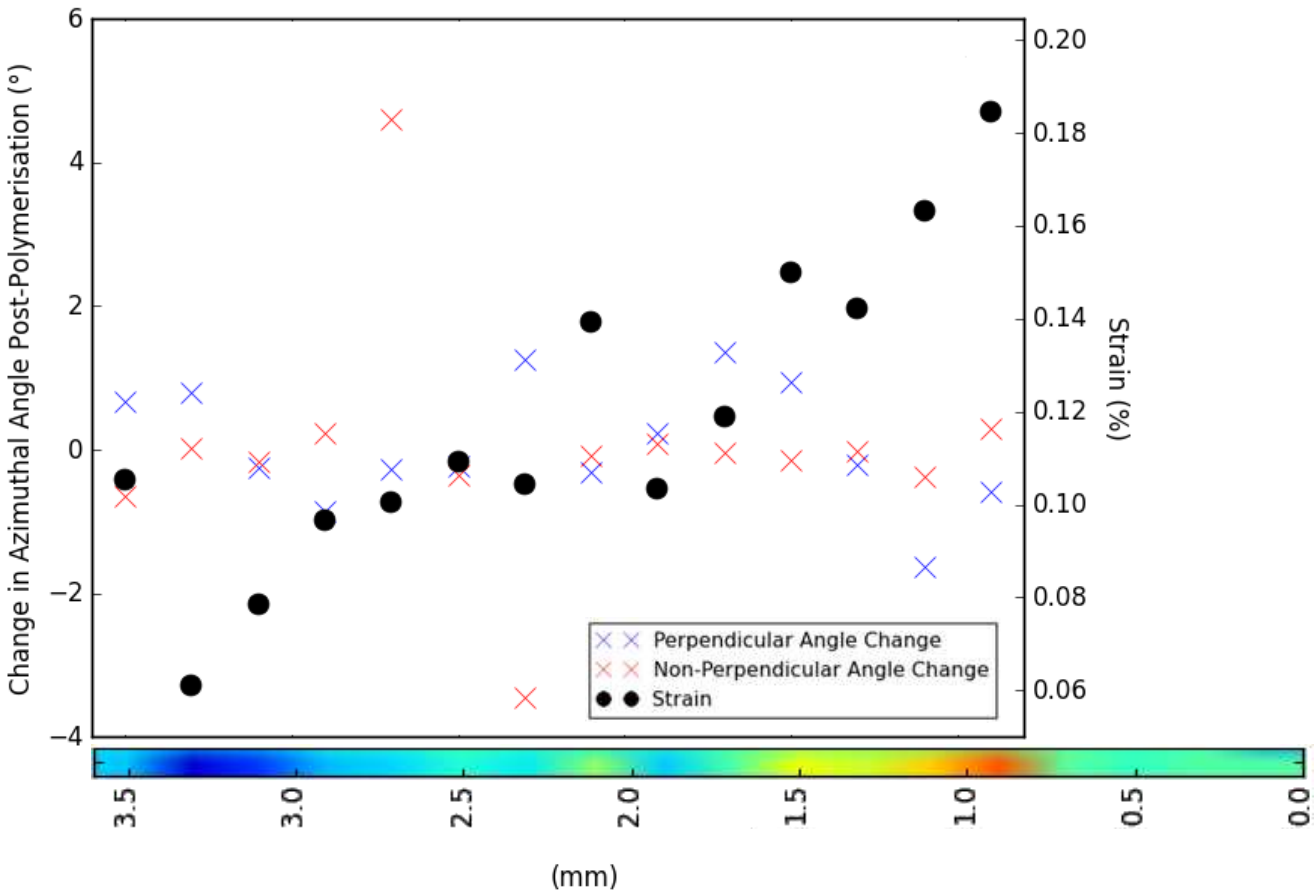

Figure 6. Changes in crystallite orientation angle post-polymerisation, for the perpendicular (blue) and non-perpendicular (red) angle directions, plotted as a function of track position with strain in the c lattice overlaid (black). A representative line track of strain in the c axis (Figure 4c, track 1) is shown beneath the plot for clarity, forming the x axis. No relationship between strain magnitude and the change in angle for the perpendicular and non-perpendicular distributions was observed. Data was not taken along the full track length as towards the tooth edge crystallites are known to be oriented normal to the tooth surface and not the cavity wall. Including this data would artificially lower the correlation between crystallite orientation and strain generated near the cavity.

Figure 7

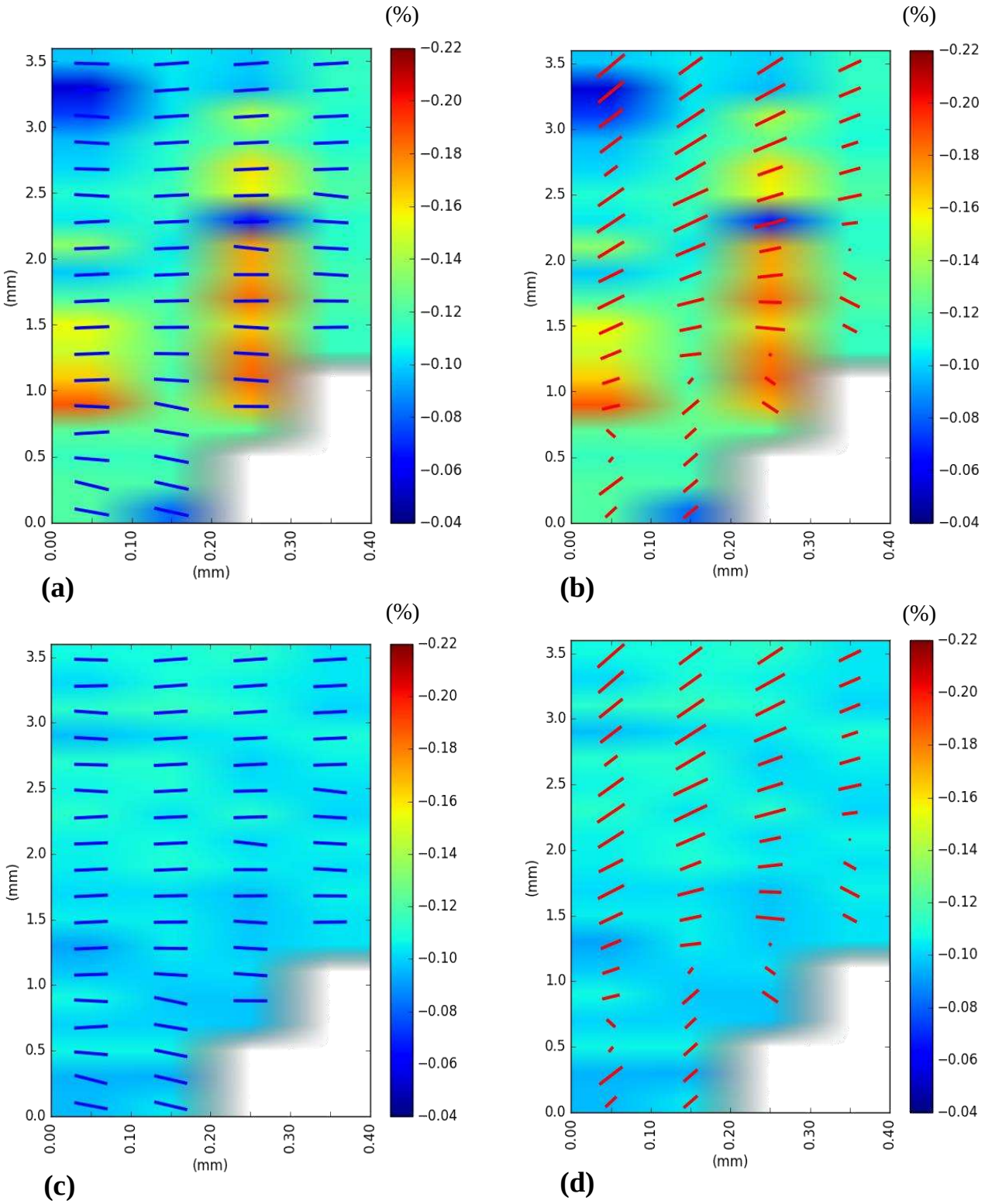

Figure 7. Orientation directions and the relative proportions of the perpendicular and non-perpendicular crystallite populations (blue and red bars respectively) overlaid on to strain data for the c (**(a)** and **(b)**) and a axis (**(c)** and **(d)**). The red bars have been scaled in length by a factor of three and the aspect ratio of the underlying strain maps have been altered for clarity.

Figure 8

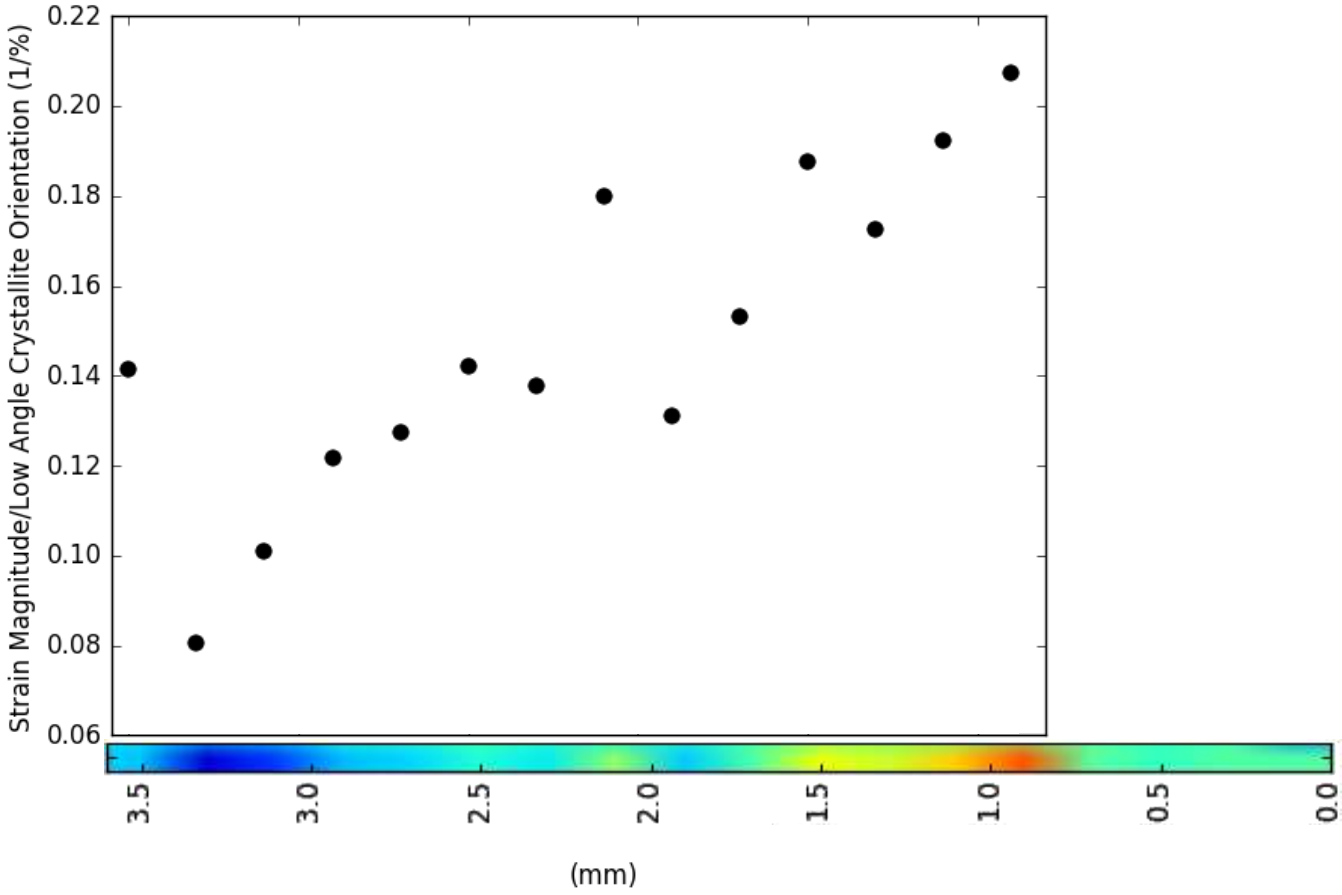

Figure 8. Ratio of the magnitude of the c axis strain to the perpendicular angle orientation population percentage as a function of track position. A corresponding line track of strain in the c axis is shown beneath the plot for clarity, forming the x axis, taken from Figure 4c (track 1). Data was not taken along the full track length as towards the tooth edge crystallites are known to be oriented normal to the surface and not the cavity wall. Including this data would artificially lower the correlation between crystallite orientation and strain generated near the cavity.